

<https://doi.org/10.1038/s43247-024-01503-7>

Extraordinary 2021 snowstorm in Spain reveals critical threshold response to anthropogenic climate change

Check for updates

Damián Insua-Costa ^{1,2} , Marc Lemus-Cánovas ^{2,3}, Juan J. González-Alemán⁴,
Martín Senande-Rivera ², María del Carmen Llasat ⁵, Gonzalo Miguez-Macho ² &
Diego G. Miralles ¹

Attribution of extreme weather events to anthropogenic climate change (ACC) has become an increasingly important line of research in recent years. However, the potential influence of ACC on heavy snowstorms remains largely unexplored. Here we focus on studying the exceptional January 2021 snowfall event in Spain, known as Filomena. First, using observational data and flow analogs, we show that the characteristic synoptic pattern leading to the episode has not significantly changed in frequency over the past decades. Based on this, we assume a fixed dynamical pattern and focus on studying the influence of ACC on the thermodynamics of the event using an atmospheric model and a storyline attribution approach. Our simulations indicate that in northern highlands, ACC intensified snowfall by up to +40% compared with pre-industrial conditions, while in nearby southern lowlands ACC weakened snowfall by up to –80%. This characteristic shift from weakening to intensification is well defined by a critical threshold in temperature. Furthermore, we show that if Filomena were to occur at the end of the 21st century, this contrasting response to ACC would be enhanced. Altogether, our findings highlight the large but uneven impact of global warming on extreme snowstorm events.

Between January 6 and 10, 2021, a low-pressure system named Filomena by the Spanish National Meteorological Service (AEMET) hit Spain, causing an extraordinary snowfall episode. In the capital, Madrid, as well as in other regions of central and eastern Iberia, the snow depth exceeded 50 cm, making it one of the worst snowstorms in recent times¹. Such snow accumulations caused widespread chaos, especially in the central part of the country, including the closure of airports and roads. Five people died and damages amounted to €1.8 billion (2021 USD2.2 billion)². In addition, the snowfall severely affected tree cover in the epicenter of the event³.

In the days and weeks following the event, many Spanish media outlets hypothesized a possible link between the Filomena snowstorm and global warming. In fact, some sectors of society adopted this hypothesis as true, interpreting the event as a sign of the dramatic impact of climate change in Spain. This is clearly palpable in the internet appearance of the term “Filomena” accompanied by “climate change”, which skyrocketed in the immediate aftermath of the event, and continued ever since (Supplementary Fig. 1). However, did anthropogenic climate forcing really promote or intensify the snowfall episode? In the past, several authors have tried to

answer this same question for extreme rainfall events^{4–7} using different climate change attribution techniques. However, attribution studies are much less numerous for extreme snowfall episodes^{8,9}, and even more so in Spain, where the attribution of extremes to anthropogenic climate change (ACC) is still underexplored.

The hypothesis that the snowstorm was to some extent linked to ACC is generally based on two main arguments. The first relates to atmospheric dynamics: according to some previous studies, the enhanced warming of the Arctic relative to lower latitudes, the so-called Arctic amplification, could lead to a wavier Northern Hemisphere jet stream¹⁰, which in turn would affect mid-latitude weather making cold air outbreaks or Filomena-like events more likely^{11–13}. The second argument is more related to atmospheric thermodynamics than dynamics: a warmer atmosphere can hold more moisture, ~7% more per degree according to the Clausius–Clapeyron relation, which could intensify snowfall if the temperature remained low enough so that precipitation did not change phase^{14–16}. However, other authors suggest that there is no significant impact of ACC on the jet stream^{17,18} and that temperature increases have only reduced snow¹⁹,

¹Hydro-Climate Extremes Lab, Ghent University, Ghent, Belgium. ²CRETUS, Non-Linear Physics Group, Universidade de Santiago de Compostela, Santiago de Compostela, Spain. ³Andorra Research + Innovation, Andorra la Vella, Andorra. ⁴Agencia Estatal de Meteorología (AEMET), Madrid, Spain. ⁵GAMA, Department of Applied Physics, Universitat de Barcelona, Barcelona, Spain. e-mail: damian.insuacosta@ugent.be

including extreme snowfall^{20,21}. In other words, although the hypothesis of an ACC influence on the Filomena snowstorm is well-founded, it is far from proven. Therefore, our main goal is to unravel the link between global warming and this extreme event, considering both dynamic and thermodynamic drivers.

When attributing extremes to ACC, probabilistic or risk-based attribution methodologies have been among the most widely used^{4,22} and, generally speaking, they consist in analyzing the change in the probability of occurrence of a particular event between different climate model scenarios. However, the ability of such models to simulate snow—especially extremes—is low and the partitioning of hydrometeors is very uneven among them²³, making them unsuitable for our case. For this reason, here we use a novel approach, based on the combination of the circulation analogs technique^{24,25} and a storyline attribution tool²⁶ in a common framework²⁷. The analogs are used to analyze whether the large-scale atmospheric pattern that led to the snowfall event has become significantly more or less frequent with warming. Faranda et al.²⁸ recently analyzed the Filomena case using this same technique; however, they did not focus on dynamics, i.e., on investigating whether the probability of such atmospheric pattern has changed. Finally, we used Pseudo Global Warming (PGW) simulations²⁹, a type of storyline attribution approach, to analyze whether global warming increased, decreased, or had no effect at all on snowfall amounts (i.e., the intensity of the event). The PGW approach focuses on the thermodynamics of the event

and has been widely used for ACC attribution of hurricanes^{30–33}, and recently also for heat waves, droughts, or extreme convective events^{34–36}. However, to the best of our knowledge, only a couple of studies have applied this technique to extreme snowfall events^{8,9}. While the region of study in those investigations was different from ours, their findings could be informative for cases like Filomena, if it was not for their contradictory results regarding the weakening or intensification of extreme snowfall following ACC. This underscores the need to continue exploring the relationship between global warming and extreme snowfall.

Results

Brief description of the event

Storm Filomena formed in the eastern U.S. as an extratropical cyclone between January 1st and 2nd (2021), and by January 3rd, it entered the Atlantic via Nova Scotia. On January 5th, it was positioned near the Azores. The storm intensified upon reaching warmer waters, causing heavy rains and winds in the Canary Islands from January 6th to 7th. Meanwhile, the Iberian Peninsula had been experiencing extreme cold since Christmas 2020. When Filomena arrived there on January 8–9th, associated with a mid-latitude trough (Fig. 1a), the combination of the warm and moist air mass transported by the storm with the pre-existing cold conditions (Fig. 1b) led to widespread snowfall, especially in the center and east of Spain (Fig. 1c, d). In addition to the snow, extreme rainfall affected southern areas of the country, such as

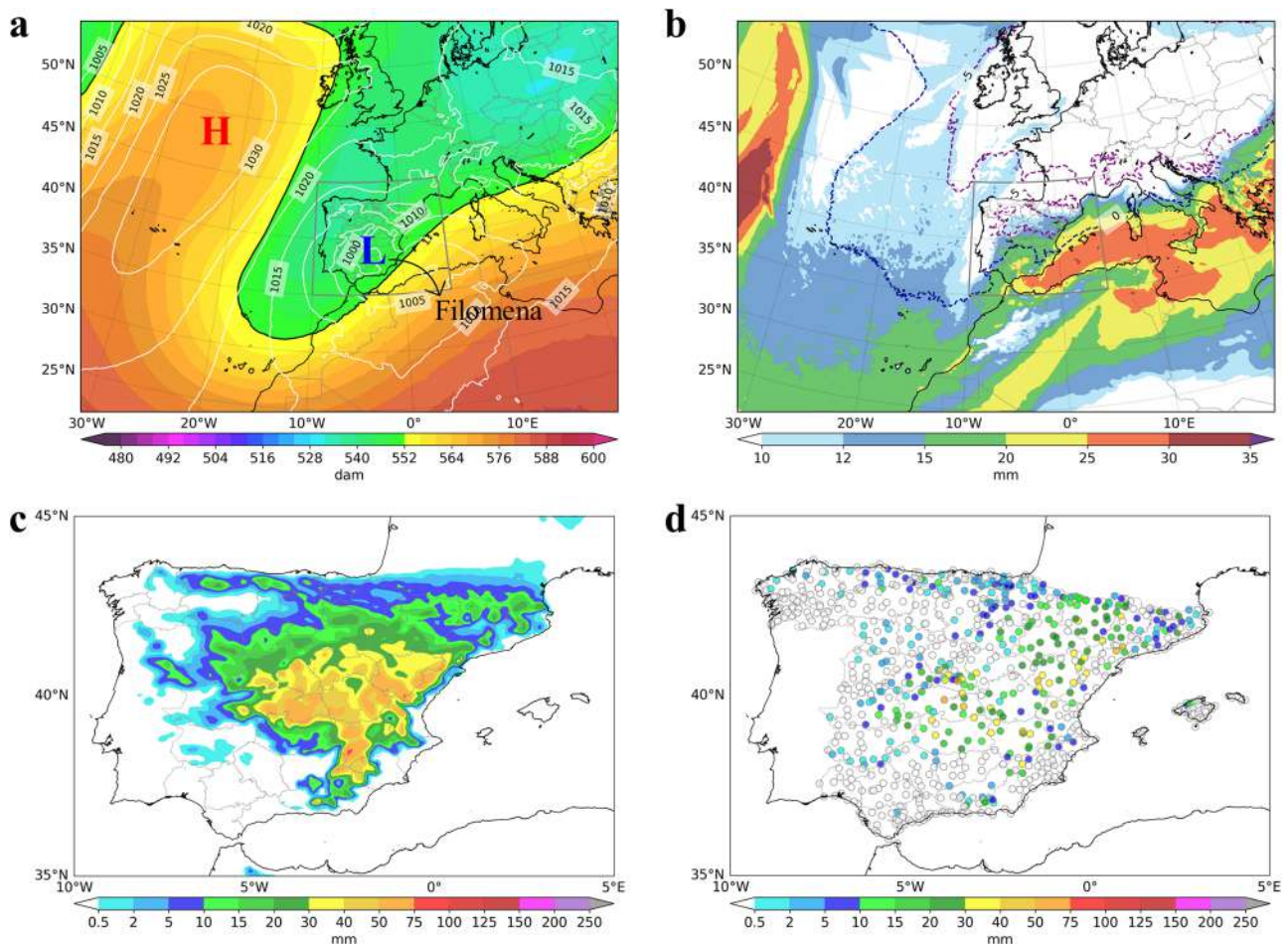


Fig. 1 | Synoptic situation and model performance. **a** Geopotential height at 500 hPa (shades in dam) and sea level pressure (white contours in hPa) simulated by the WRF model at 00UTC on January 9, 2021. The letters L (blue) and H (red) indicate the central position of the low- and high-pressure systems at that instant, respectively. **b** Total precipitable water (shades in mm) and isotherms of 0 °C and -5 °C at 850 hPa (dashed dark blue and purple contours, respectively) for the same

model and instant as (a). **c** Snow water equivalent simulated by WRF for the 3 main days of the event (from 00UTC January 7 to 00UTC January 10). **d** Same as (c) but for observed snow from AEMET weather stations. The gray boxes in (a, b) indicate the region selected to show the snowfall fields in (c, d), roughly corresponding with the Iberian Peninsula domain. The simulated fields in (a, b, c) correspond to the average of all WRF ensemble members.

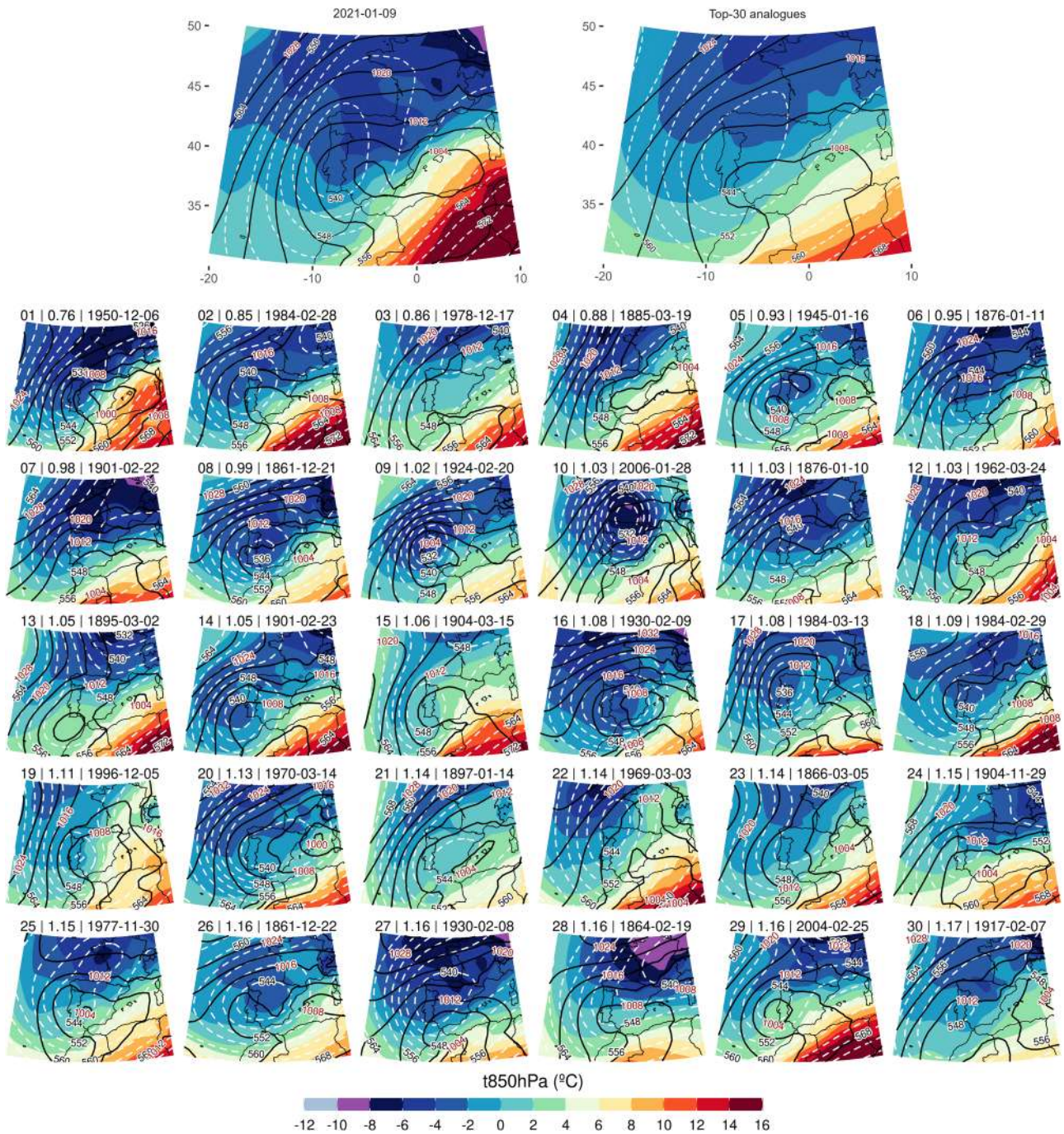


Fig. 2 | Filomena-like storms. The 30 closest flow analogs to Filomena since 1836 in terms of geopotential height at 500 hPa (dashed white contours in dam) and sea level pressure (black contours in hPa). Analogs are ordered according to the cumulative normalized RMSD for both variables (shown to the left of the date above the figures), so that analog 1 (top left) would be the closest to Filomena. The temperature at

850 hPa (shades in °C) is also plotted, even though it was not used in the search for analogs. Note that the reference pattern, i.e., the mean fields for the main day of the event, 9 January 2021, is shown at the top (left), together with the averaged fields for the 30 analogs shown (right).

Malaga in Andalusia, with more than 250 mm accumulated between 7 and 11 January in some places¹. Finally, the aftermath of Filomena led to a remarkable cold wave from 11 to 17 January, setting new temperature records with lows reaching -26.5°C in some areas¹. For a better understanding of the time evolution of the conditions leading to the event, see Supplementary Fig. 2, which shows the same fields in Fig. 1a, b for different days of the event.

Figure 1c, d show the snowfall (in terms of snow water equivalent, not snow depth) simulated by the Weather Research and Forecasting (WRF) model with which the PGW simulations were carried out (see Methods section), and that observed at different weather stations of the AEMET

network, respectively. The WRF simulations (Fig. 1c) are able to capture the strong snowfall event and its geographical distribution. Despite differences in specific locations, the model simulates well the observed snowfall pattern (Fig. 1d), with maximum values over the centre of the Iberian Peninsula extending eastwards. Most importantly, in places where the snowfall was most severe, the model predicted values of $\sim 30\text{--}50$ mm in agreement with the in situ observations. Furthermore, it is important to note that snow water equivalent observations are far from perfect; thus differences between simulation and observations in some areas do not necessarily indicate model errors. In Supplementary Fig. 3 we show an additional validation of the

model results, comparing the simulated synoptic situation (Fig. 1a) and the simulated snowfall (Fig. 1c) against reanalysis data, which further supports the accuracy of the model results.

Filomena-like storms and their long-term frequency trend

As stated in the Introduction, a possible connection between ACC and the Filomena snowstorm could arise from a change in atmospheric dynamics eventually increasing the frequency of this type of event. To test this hypothesis, we detected all historical circulation analogs (from 1836 to 2015) considering the geopotential height at 500 hPa and sea level pressure (see Methods for details). In Fig. 2 we show the 30 closest analogs to Filomena (i.e., those minimizing the cumulative normalized RMSD of both variables). The similarity between the analogs and the case study is evident when they, or their average (top right in Fig. 2), are compared to the actual atmospheric pattern leading up to the event, i.e., the ERA5 reference fields used for the analogs experiment (top left in Fig. 2). In fact, some of the analogs coincide with historical snowfall events in the central part of the Iberian Peninsula, such as that in February 1984 (position 2) or that in November 1904 (position 24). This shows that the atmospheric configuration of Filomena entails a high risk of severe snowfall in the area and that the method used to detect analogous events is effective.

In Fig. 3 we represent the time series of all analog days per year, ranging from 0 to 6 days, with point maxima of 9 days. The slope of the linear regression of the analog frequency (red line in Fig. 3) reveals that there is no significant long-term trend ($p > 0.05$). In this figure, we also show the frequency per decade (upper right corner) which clearly evidences that there is no clear trend. Therefore, we discard the hypothesis that ACC has increased the frequency of this type of synoptic configuration in any significant way. In other words, based on these results, if ACC had affected the snowfall event it would have been through changes in atmospheric thermodynamics and not dynamics.

ACC influence on Filomena snowfall intensity

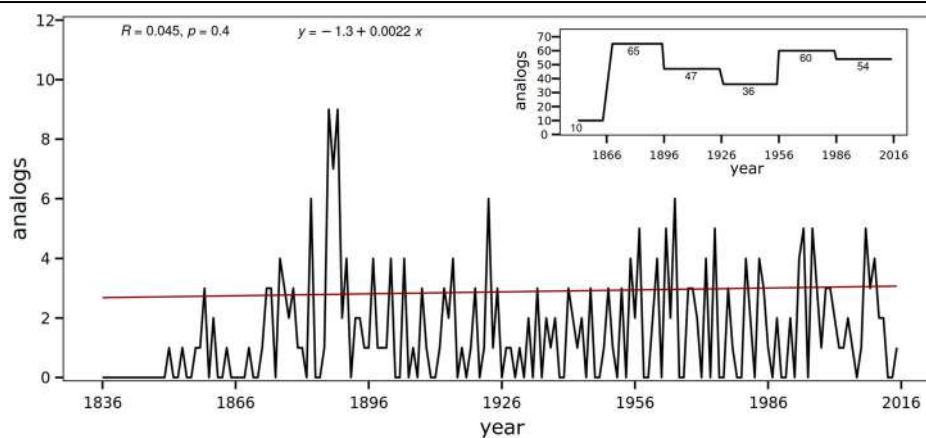
To assess the influence of ACC on the huge snowfall amounts recorded, we compared the simulated snowfall for the Filomena event in the counterfactual simulations (Supplementary Fig. 4) with the factual simulations (Fig. 1c). As better explained in the Methods section, both counterfactual simulations for the past (pre-industrial era) and for the future (2070–2100) are based on WRF perturbed with the anthropogenic climate signal extracted from different CMIP6 models. Figure 4a shows the mean difference in snow water equivalent between the present and the pre-industrial past. In addition, in Fig. 4b we show the simulated snow water equivalent values for three specific cities: Soria, Madrid, and Ciudad Real, indicated with a 1, 2, and 3 in Fig. 4a, respectively. These box-plots show the values for both the past (purple) and present (blue) counterfactual simulations and allow us to appreciate the dispersion between the different members of the ensemble described in Methods. Finally, Fig. 4c shows the relative difference

in snow between present and past for these three cities. Therefore, positive values in both Fig. 4a (in green and blue colors) and 4c indicate more snow in the present than in the past. Analogously, Fig. 4d, e, f analyze the differences in snow water equivalent between simulations for the future (red in Fig. 4e) and those for the present (blue in Fig. 4e). In this case, the positive values in Fig. 4d, f indicate more snow in the future scenario than in the present climate, i.e., in reality.

Given that in both present versus past and future versus present simulations there is a generalized increase in temperature, higher for the future (see Supplementary Fig. 5a, b), the first thing standing out is that warming has an uneven effect on recorded snowfall amounts. In the north-northwestern areas, warming tends to intensify snowfall, with increases of up to +7 mm in the present versus the past (Fig. 4a) and exceeding +15 mm in some areas for the future versus the present (Fig. 4d). However, in the south and southeast, warming tends to weaken the snowfall, with decreases in excess of -30 mm, more widespread in the future versus the present (Fig. 4d) than in the present versus the past (Fig. 4a). Absolute differences in snowfall between the present climate and the pre-industrial past yield weakening and intensification values of up to -80% and +40% when analyzed in relative terms, respectively (Supplementary Fig. 6). For the differences between the future scenario and the present climate, these relative differences intensify, with large areas where snowfall disappears (-100%) and others where it intensifies by more than +60%. Despite this uneven pattern, weakening prevails over intensification, which means that both the area affected by snowfall and the total snow amount decrease with warming when analyzing the region as a whole (see Supplementary Table 1).

When we focus on the 3 cities mentioned above, this differing pattern is clearly reflected; in fact, the selection of these three cities and not others was intended to show precisely this pattern. In Soria, the northernmost city, the amount of snowfall goes from 12 mm in the pre-industrial past to 14 mm in the present climate (Fig. 4b) and about 19 mm in the future (Fig. 4e), which is equivalent to relative increases of about +15% (Fig. 4c) and +35% (Fig. 4f). Conversely, in Ciudad Real, the southernmost city, snowfall goes from almost 35 mm in the pre-industrial past to just over 15 mm in the present (-50%) and 0 mm in the future (-100%). For both cities, although the different ensemble members show an important dispersion, the signs of the relative change (positive in Soria and negative in Ciudad Real) are highly significant ($p < 0.001$). Madrid, however, is located in the center of the Iberian Peninsula and is therefore around the limit between the zone of snowfall intensification in the north and the zone of weakening in the south. On average, the simulations show that the snowfall was slightly more intense in the present than it would have been in the pre-industrial past, increasing from 46 to 48 mm (+5%), but the statistical significance of this change is lower ($0.01 < p < 0.05$). For the future, there is a higher degree of certainty ($p < 0.001$) that Madrid would move into the weakening zone, so that snowfall amounts would be reduced by more than -10% (from 48 to 42 mm). Note that a more detailed analysis of the uncertainty can be found

Fig. 3 | Historical evolution of the frequency of Filomena-like storms. Number of Filomena flow analogs per year (black line) and their long-term trend (red line). The correlation coefficient (R), the p value (p) and the equation of the straight line used in the regression are shown at the top left. The plot in the upper right corner shows the number of analogs per decade.



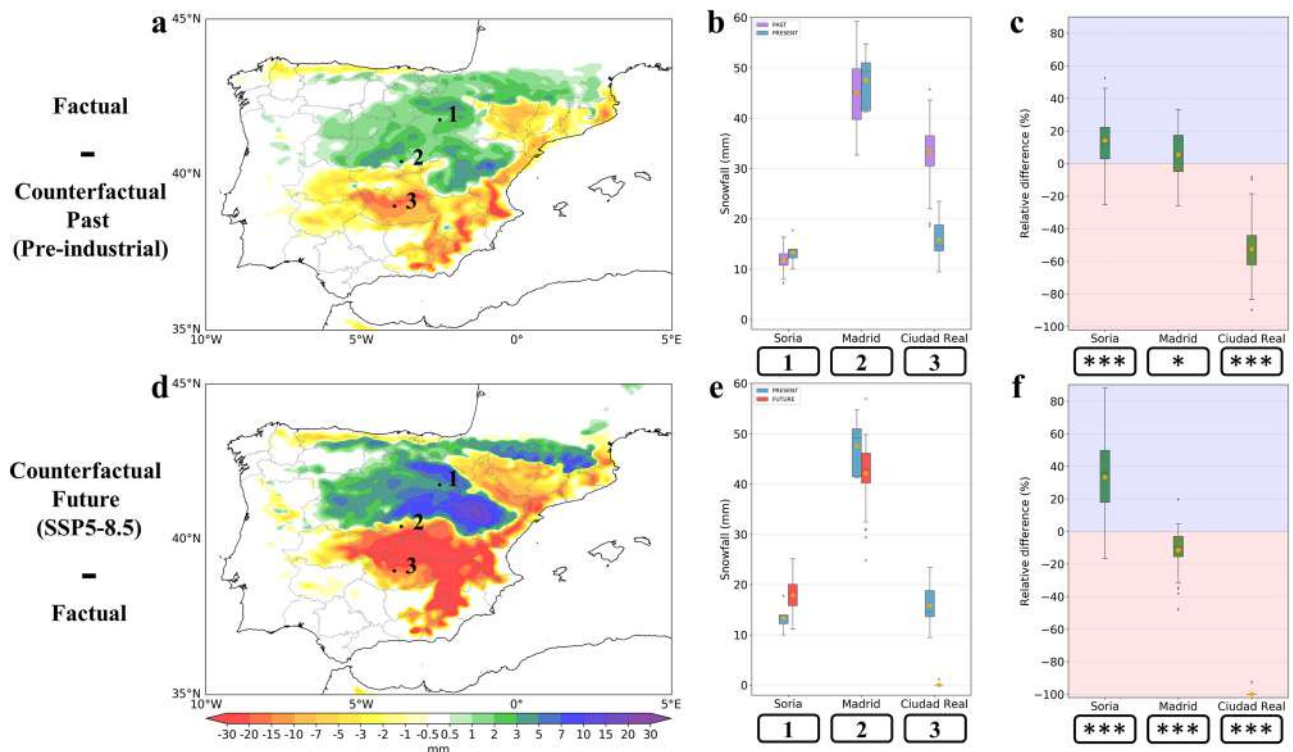


Fig. 4 | Changes in Filomena’s intensity. **a** Difference in accumulated snow water equivalent for the main days of the event (from 00UTC January 7 to 00UTC January 10) between the mean of all factual simulations and the pre-industrial counterfactual ones. **b** Snow water equivalent for three Spanish cities (Soria, Madrid, and Ciudad Real) indicated with a number in **(a)** (1, 2, and 3, respectively). Snowfall amount is shown for both past (purple) and present (blue) climates. The box-plots show the dispersion between the different simulations performed, with the orange dot

highlighting the ensemble mean. **c** Relative difference in snow water equivalent between past and present climate for the three cities. Asterisks show the level of statistical significance (one asterisk $p < 0.05$, 2 asterisks $p < 0.01$ and three asterisks $p < 0.001$). This is calculated using a t-test, with the null hypothesis being that the relative change in snow is zero. **d, e, f** Same as **(a, b, c)** but for the mean difference between snow water equivalent in the future counterfactual simulations (SSP5-8.5 scenario) and the factual ones.

in Supplementary Fig. 7, where the relative changes in snowfall in these three cities are shown for all members of our ensemble.

To better understand the spatial pattern of change in snowfall with warming depicted in Fig. 4, in Fig. 5 we show the relative differences in terms of snow water equivalent, both for present versus past (Fig. 5a), and future versus present (Fig. 5b), as a function of latitude (Y-axis) and altitude (X-axis). We also show these relative variations for total precipitation and not just snowfall (Fig. 5c, d). From Fig. 5a, b, we can robustly conclude that snowfall tends to intensify in high-elevation and high-latitude areas while decreasing in low-elevation and low-latitude regions. In fact, that the difference in snowfall between counterfactual and factual scenarios depends on elevation is already evident when comparing these fields (Fig. 4a, d) with the topography of the region (Supplementary Fig. 8). Total precipitation, however, intensifies almost everywhere due to the generalized increase in total precipitable water expected from the Clausius–Clapeyron relation (see Supplementary Fig. 5c, d), although there still remains a small dependence on latitude. In view of these figures, the reason behind the pattern of variation in snowfall is evident; in those places where, despite the warming, the temperature is still low enough for precipitation to remain in snow form (such as in northern and/or highland areas) snowfall intensifies because of the increase in atmospheric moisture. However, in lower elevations and especially in the south, warming is sufficient to bring the temperature above the freezing point for part or all of the event’s duration, so that despite the increase in total precipitation, the snowfall diminishes as a result of the phase change to liquid.

Discussion

Our findings show a complex response of the Filomena snowstorm to ACC. Although the frequency of the synoptic configuration that triggered the event did not increase with warming, it did significantly affect the snowfall

intensity and spatial distribution through thermodynamic influences. The spatially heterogeneous response of the event to ACC is clearly reflected in the fact that for some places the temperature increases since pre-industrial times was sufficient to reduce snowfall amounts by up to -80% , while in others (in the order of 100 km apart), even in a future scenario of extreme warming, snowfall would intensify by more than $+60\%$.

The contrasting pattern of ACC influence is a consequence of the combined effect of both an increase in air temperature and humidity on snowfall, something that has already been proposed by other authors in the past. For example, it is known that climate models simulate an increase in snowfall in polar latitudes, where the mean temperature is below a critical threshold according to previous studies^{14,15,21}. Climate models also simulate this same effect of intensified snowfall in high mountain areas^{20,37}. However, in warmer areas, and especially in those with an average temperature close to the melting point, snowfall is expected to be drastically reduced³⁸. Our analysis based on recent snow reanalysis data confirms this response of snowfall to warming. Specifically, using ERA5 data from 1941 to 2022, we calculate that, considering the period from October to March, the critical threshold marking the separation between increase and decrease of snowfall in the Northern Hemisphere corresponds approximately to the $-5\text{ }^\circ\text{C}$ isotherms (Fig. 6 right). Therefore, this threshold effect, which had already been demonstrated at the climatological scale (decades), also applies at the local or event scale (a few days). In other words, just as at the climatic scale there is a limit marked by a given isotherm, usually close to polar areas or very high mountain systems, beyond which the annual snowfall goes from decreasing to intensifying, at the event scale there is also a very clear boundary beyond which the same effect occurs (Fig. 6 left). In the case of Filomena this critical threshold of approximately $-1\text{ }^\circ\text{C}$ was located at an altitude close to that of Madrid ($\sim 657\text{ m.a.s.l.}$). Although the threshold was somewhat variable with latitude, it shows that at the event scale, the

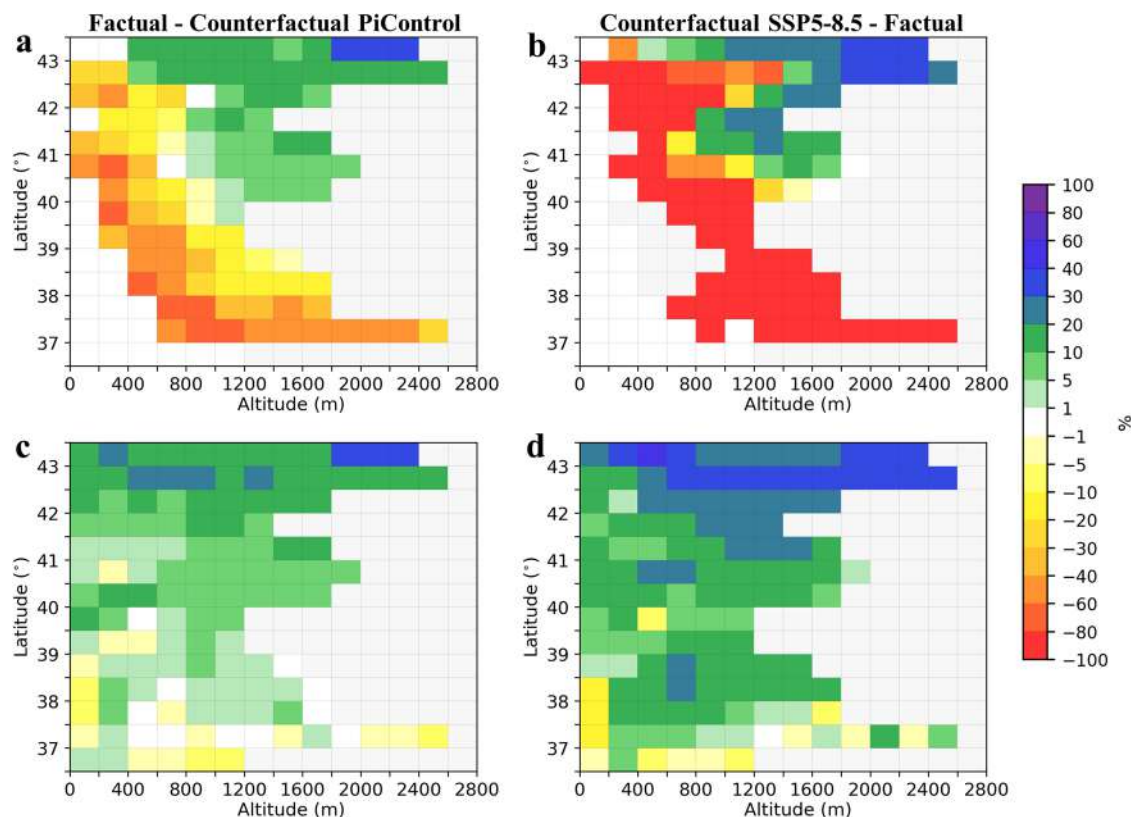


Fig. 5 | Drivers for the change in the spatial pattern of snowfall. **a** Relative difference in snow water equivalent between the mean of all factual simulations and the pre-industrial counterfactual ones according to altitude (X-axis) and latitude (Y-axis). The values are the averages of all grid cells in the simulation domain falling

between -9.5 and 3.5° longitude (roughly matching the Iberian Peninsula) clustered by altitude and latitude. **b** Same as **(a)** but for the mean difference between future counterfactual simulations (SSP5-8.5 scenario) and factual ones. **c**, **d** Same as **(a**, **b)** but for total precipitation, not just snow.

boundary between weakening and intensification of snowfall may not be located particularly far north or at particularly high elevations, as is the case for the climatic scale. The position of this boundary also depends on the nature of the event; if the Filomena cyclone had advected colder air from the northern regions, it would have been lower, both in altitude and latitude. The integration of different snow events over time (schematized with the overlapping panels on the left in Fig. 6) ultimately determines the critical threshold at a climatic scale (Fig. 6 right).

Our analysis focuses on a single case, but the results obtained can be extrapolated to other extreme snowfall events, since the conclusions reached are based on basic thermodynamical principles. This allows us to propose a general rule about the effect of ACC (from the thermodynamic point of view) on a given snowfall event, based on four possible scenarios: (1) if the current (factual) temperature is clearly above the freezing point, there is no change because, even if it was colder in pre-industrial times, the temperature would still not be low enough for snowfall to occur (neither snow in the past nor in the present). (2) If the temperature is close to but above freezing, it is very likely that ACC has greatly diminished snowfall, or made it disappear altogether, since the temperature increase since pre-industrial times has been sufficient to change the precipitation phase to liquid. (3) However, if the temperature is close to but below the freezing point, it is likely that ACC has had little effect or even reduced snowfall. This is because although the average temperature is negative, being close to the freezing point, it is to be expected that during part of the episode the temperature will be positive and the precipitation will be in liquid form. In this case the intensity of the snow would increase but the duration would decrease compared to the pre-industrial era, compensating each other. For the Filomena event, this would be the case for areas with mean temperatures between 0 and -1°C (the critical threshold). (4) Finally, if the current temperature is well below freezing, we can conclude that the ACC is having the opposite, snowfall

enhancing effect, because in this case the temperature is still low enough for snow occurrence and the increase in atmospheric moisture induced by warming intensifies precipitation. This four-case rule is visually interpreted in Supplementary Fig. 9.

To conclude, based on our results and given the very high media and social interest generated by this case (Supplementary Fig. 1), when faced with a Filomena-like episode, we ask that hypotheses or even statements linking it with ACC be cautious and consider the particularities of this type of extreme weather events.

Methods

Filomena flow analogs

We employed the flow analog technique, commonly used in ACC attribution studies^{24,25,28}, to find similar dynamic configurations to the one that led to Filomena. Analogous days were selected in a restricted domain spanning coordinates from 20°W to 8°E in longitude, and from 29.5°N to 55°N in latitude, which allowed capturing the main circulation features associated with the event. In the experiment, we jointly used the daily mean sea level pressure (MSLP) and geopotential height at 500 hPa (Z500), both previously normalized, from the 20th Century Reanalysis³⁹ (20th-CR.V3) at 1° spatial resolution from November to March and for the period from 1836 to 2015. In addition, we used the 5th generation of the European Centre for Medium Range Weather Forecasts (ECMWF) global reanalysis (ERA5⁴⁰) to define the Z500 and MSLP fields of the reference atmospheric pattern—normalized using 20th-CR.V3 as the base time series—i.e., that of the average of the main day of the event (January 9, 2021). To select the analog days, we employed root mean square differences (RMSD) to calculate the distances between our predictand (Filomena reference atmospheric pattern) and the potential analogs between 1836 and 2015 from the 20th-CR.V3. Specifically, we consider the cumulative RMSD of both normalized variables

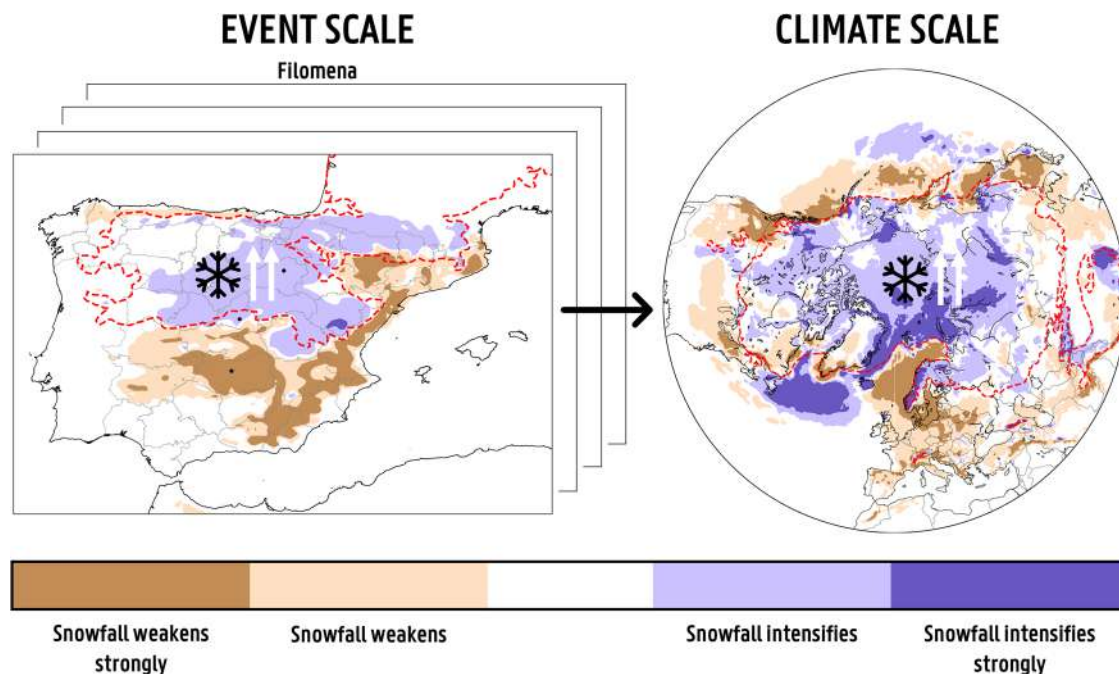


Fig. 6 | Snowstorms response to global warming. At a local or event scale, our study shows that snow events respond to temperature increase similarly to how snow does at a climate scale. On the left, we show the difference in snowfall for the Filomena event between WRF simulations for the present and for the past (same as Fig. 4a). On the right we show the difference between snowfall in the period 1982–2022 and 1941–1981 based on ERA5 reanalysis data. For the event scale (left), intensification and strong intensification mean increases in snowfall above 1 mm and 5 mm for the main days of the event (from 00UTC January 7 to 00UTC January 10), respectively.

Weakening and strong weakening mean the opposite. For the climate scale (right) these values correspond to \pm mm/year and \pm 20 mm/year. The dashed red lines show the critical thresholds that separate the zones of intensification and weakening of snowfall. In the case of Filomena it is defined using the mean temperature on the main days of the event (calculated from WRF factual simulations) and corresponds to the -1 °C isotherm. For the climatic scale, it is defined using the October–March average temperature from ERA5 in the period from 1941 to 2022 and is estimated as -5 °C.

(Z500 and MSLP). The closest 1% of the 27,218 candidate days in the 20th-CR.V3 were retained as the final analogs, resulting in a set of 272 flow analogs for the Filomena event in the 180-year period. With the finally selected analogs, we computed the top-30 ranking of historical synoptic composites closest to the Filomena case (those minimizing the cumulative RMSD of Z500 and MSLP)—see Fig. 2. In addition, we computed annual counts of analogs between 1836 and 2015, as well as time series, aggregated over 30-year-long periods (Fig. 3). Finally, we estimated the long-term trend of the annual analog time series using linear regression, and used the p value of a t -test to evaluate the statistical significance of this trend (Fig. 3).

Filomena storylines

We simulated the event in the current climate (hereafter, factual simulation), as well as in pre-industrial and future climates (hereafter counterfactual past and future simulations, respectively), using the WRF regional atmospheric model v4.2.2⁴¹. For the counterfactual simulations, we perturb both initial and boundary conditions of the model, from ERA5⁴⁰, following the PGW approach²⁹. This means that the perturbation is intended to account for the ACC forcing on the thermodynamical variables associated with the event. Specifically, we perturb only purely thermodynamic variables, including 2 m temperature and dewpoint temperature, skin temperature, sea surface temperature, air temperature and specific humidity at all vertical levels of the atmospheric column. Greenhouse gases, including CO₂, CH₄, and N₂O were also perturbed in the counterfactual simulations to match pre-industrial⁴² and expected future⁴³ concentrations of these gases (see Supplementary Table 2). Mathematically:

$$\chi_c = \chi_f + \chi_a \tag{1}$$

Where χ_c stands for the counterfactual initial and boundary conditions in one of the perturbed variables, χ_f would be the factual variable and χ_a the

anthropogenic forcing calculated as:

$$\begin{cases} \chi_a^{past} = \chi_{piC}^{CMIP6} - \chi_{hist}^{CMIP6} \\ \chi_a^{future} = \chi_{SSP}^{CMIP6} - \chi_{hist}^{CMIP6} \end{cases} \tag{2}$$

Where χ_a^{past} and χ_a^{future} are past and future ACC forcings on a variable of interest, respectively, χ_{piC}^{CMIP6} is the 500-year mean of this variable in the pre-industrial control (piC) simulation of a CMIP6⁴⁴ climate model, χ_{hist}^{CMIP6} is the mean of the variable in the historical (hist) simulations and χ_{SSP}^{CMIP6} is the mean for a specific shared socioeconomic pathway (SSP) future scenario. In our case, we use a high emission scenario (SSP5-8.5) to assess the future maximum potential changes in the snowstorm. It should be noted that since χ_{hist}^{CMIP6} is in principal intended to account for the current climate, and the event occurred in 2021, we had to concatenate it with the CMIP6 climate model simulation for an intermediate pathway (2006–2014 from the historical experiment and 2014–2036 from the SSP2-4.5 scenario) in order to obtain a climate mean centered on 2021. For the future (χ_{SSP}^{CMIP6}) we considered the 31-year period from 2070 to 2100. To calculate these climate change forcings, we used the daily interpolated monthly data from the CMIP6 models, so that we were able to perturb each day of the event with its corresponding anthropogenic forcing for that day. This means that since the Filomena case occurred in the first half of January, the perturbations correspond to the weighted average of December and January, with the latter having more weight. The anthropogenic signals were computed separately for five different CMIP6 models (CESM2-WACCM, EC-Earth3, MPI-ESM1-2-HR, MRI-ESM2-0 and NorESM2-MM). These models were selected because they are the ones that can separately provide all the variables to be perturbed in the PGW simulations, which were introduced above, and for all the climate scenarios considered. Other models can also provide them but at lower resolution (>100 km) so we discarded them.

Moreover, between the five of them they cover a wide range of possible climate sensitivities (see Supplementary Table 1), which makes them particularly suitable for assessing the uncertainty of our results.

The WRF simulations were performed at a resolution of 9 km in a domain roughly centered in Spain and covering much of the North Atlantic and Europe (see Fig. 1a, b). Since we started the simulations several days before the event (starting at 00UTC on January 4), we used a spectral nudging technique⁴⁵ to prevent the large-scale dynamics from drifting away from those in the ERA5 reanalysis. Finally, we tested 8 different physical configurations of the model (see Supplementary Table 3). Considering that we also used five different CMIP6 models, this means that we built an ensemble of 40 simulations for both past and future climate (i.e., 8 physical configurations × 5 CMIP6 model perturbations), which allows us to estimate the uncertainty of the results. The simulations in the present climate are obviously not affected by the perturbations of the climate models, so they only form an ensemble of 8 members, each corresponding to a different physical configuration. Thus, in Fig. 1a–c, what is shown are the average fields of these 8 simulations.

Data availability

All datasets used in this study are publicly available. The ERA5 reanalysis data are available at <https://cds.climate.copernicus.eu/#/search?text=ERA5>. The 20th-CR.V3 reanalysis data are available at https://psl.noaa.gov/data/gridded/data.20thC_ReanV3.html. The simulation outputs of CMIP6 models (CESM2-WACCM, EC-Earth3, MPI-ESM1-2-HR, MRI-ESM2-0 and NorESM2-MM) are available at <https://esgf-data.dkrz.de/search/cmip6-dkrz/>.

Code availability

The WRF v4.2.2 model is available at <https://github.com/wrf-model/WRF/releases>. The flow analogs technique code is available on request from M.L.C.

Received: 12 January 2024; Accepted: 7 June 2024;

Published online: 20 June 2024

References

1. AEMET: Informe sobre el episodio meteorológico de fuertes nevadas y precipitaciones ocasionadas por borrasca Filomena y posterior ola de frío (in Spanish), accessed 18 November 2023; https://www.aemet.es/documentos/es/conocerlas/recursos_en_linea/publicaciones_y_estudios/estudios/Informe_episodio_filomena.pdf (2021).
2. AON: Global Catastrophe Recap January 2021, accessed 15 May 2023; https://www.aon.com/reinsurance/getmedia/74fc7a33-5ef9-4b2b-82fb-719ee08add29/20210209_analytics-if-january-global-recap.pdf.aspx (2021).
3. Pérez-González, M. E., García-Alvarado, J. M., García-Rodríguez, M. P. & Jiménez-Ballesta, R. Evaluation of the impact caused by the snowfall after storm filomena on the arboreal masses of Madrid. *Land* **11**, 667 (2022).
4. Pall, P. et al. Anthropogenic greenhouse gas contribution to flood risk in England and Wales in autumn 2000. *Nature* **470**, 382–385 (2011).
5. van der Wiel, K. et al. Rapid attribution of the August 2016 flood-inducing extreme precipitation in south Louisiana to climate change. *Hydrol. Earth Syst. Sci.* **21**, 897–921 (2017).
6. Risser, M. D. & Wehner, M. F. Attributable human-induced changes in the likelihood and magnitude of the observed extreme precipitation during Hurricane Harvey. *Geophys. Res. Lett.* **44**, 12457–12464 (2017).
7. Van Oldenborgh, G. J. et al. Attribution of extreme rainfall from Hurricane Harvey, August 2017. *Environ. Res. Lett.* **12**, 124009 (2017).
8. Ashley, W. S., Haberlie, A. M. & Gensini, V. A. Reduced frequency and size of late-twenty-first-century snowstorms over North America. *Nat. Clim. Change* **10**, 539–544 (2020).
9. Kawase, H., Imada, Y. & Watanabe, S. Impacts of historical atmospheric and oceanic warming on heavy snowfall in December 2020 in Japan. *J. Geophys. Res. Atmos.* **127**, e2022JD036996 (2022).
10. Francis, J. & Vavrus, S. Evidence for a wavier jet stream in response to rapid Arctic warming. *Environ. Res. Lett.* **10**, 014005 (2015).
11. Cohen, J. et al. Arctic warming, increasing fall snow cover and widespread boreal winter cooling. *Environ. Res. Lett.* **7**, 014007 (2012).
12. Liu, J. P., Curry, J. A., Wang, H., Song, M. & Horton, R. M. Impact of declining Arctic sea ice on winter snowfall. *Proc. Natl Acad. Sci. USA* **109**, 4074–4079 (2012).
13. Francis, J. A. & Vavrus, S. J. Evidence linking Arctic amplification to extreme weather in mid-latitudes. *Geophys. Res. Lett.* **39**, L06801 (2012).
14. Räisänen, J. Warmer climate: less or more snow? *Clim. Dynam.* **30**, 307–319 (2008).
15. Krasting, J., Broccoli, A., Dixon, K. & Lanzante, J. Future changes in northern hemisphere snowfall. *J. Clim.* **26**, 7813–7828 (2013).
16. Kapnick, S. B. & Delworth, T. L. Controls of global snow under a changed climate. *J. Clim.* **26**, 5537–5562 (2013).
17. Screen, J. A. & Simmonds, I. Exploring links between Arctic amplification and mid-latitude weather. *Geophys. Res. Lett.* **40**, 959–964 (2013).
18. Barnes, E. A. Revisiting the evidence linking Arctic amplification to extreme weather in midlatitudes. *Geophys. Res. Lett.* **40**, 4734–4739 (2013).
19. Bormann, K. J., Brown, R. D., Derksen, C. & Painter, T. H. Estimating snow-cover trends from space. *Nat. Clim. Chang.* **8**, 924–928 (2018).
20. de Vries, H., Lenderink, G. & van Meijgaard, E. Future snowfall in western and central Europe projected with a high-resolution regional climate model ensemble. *Geophys. Res. Lett.* **41**, 4294–4299 (2014).
21. O’Gorman, P. A. Contrasting responses of mean and extreme snowfall to climate change. *Nature* **512**, 416–418 (2014).
22. Stott, P. A., Stone, D. A. & Allen, M. R. Human contribution to the European heatwave of 2003. *Nature* **432**, 610–614 (2004).
23. Lin, W. & Chen, H. Daily snowfall events on the Eurasian continent: CMIP6 models evaluation and projection. *Int. J. Climatol.* **42**, 6890–6907 (2022).
24. Cattiaux, J. et al. Winter 2010 in Europe: a cold extreme in a warming climate. *Geophys. Res. Lett.* **37**, GL044613 (2010).
25. Stott, P. A. et al. Attribution of extreme weather and climate-related events. *Wiley Interdiscip. Rev. Clim. Change* **7**, 23–41 (2016).
26. Shepherd, T. G. et al. Storylines: an alternative approach to representing uncertainty in physical aspects of climate change. *Clim. Chang* **151**, 555–571 (2018).
27. Shepherd, T. G. A common framework for approaches to extreme event attribution. *Curr. Clim. Chang. Rep.* **2**, 28–38 (2016).
28. Faranda, D. et al. A climate-change attribution retrospective of some impactful weather extremes of 2021. *Weather Clim. Dynam.* **3**, 1311–1340 (2022).
29. Schär, C., Frei, C., Lüthi, D. & Davies, H. C. Surrogate climate-change scenarios for regional climate models. *Geophys. Res. Lett.* **23**, 669–672 (1996).
30. Lackmann, G. M. Hurricane Sandy before 1900 and after 2100. *Bull. Am. Meteorol. Soc.* **96**, 547–560 (2015).
31. Patricola, C. M. & Wehner, M. F. Anthropogenic influences on major tropical cyclone events. *Nature* **563**, 339–346 (2018).
32. Reed, K. A., Stansfield, A. M., Wehner, M. F. & Zarzycki, C. M. Forecasted attribution of the human influence on Hurricane Florence. *Sci. Adv.* **6**, eaaw9253 (2020).
33. Reed, K. A., Wehner, M. F. & Zarzycki, C. M. Attribution of 2020 hurricane season extreme rainfall to human-induced climate change. *Nat. Commun.* **13**, 1905 (2022).
34. Sánchez-Benítez, A. et al. The July 2019 European heat wave in a warmer climate: storyline scenarios with a coupled model using spectral nudging. *J. Clim.* **35**, 2373–2390 (2022).

35. van Garderen, L. & Mindlin, J. A storyline attribution of the 2011/2012 drought in Southeastern South America. *Weather* **77**, 212–218 (2022).
36. González-Alemán, J. J. et al. Anthropogenic warming had a crucial role in triggering the historic and destructive Mediterranean derecho in summer 2022. *Bull. Am. Meteorol. Soc.* **104**, E1526–E1532 (2023).
37. Rasmussen, R. et al. High-resolution coupled climate runoff simulations of seasonal snowfall over Colorado: a process study of current and warmer climate. *J. Clim.* **24**, 3015–3048 (2011).
38. Brown, R. D. & Mote, P. W. The response of Northern Hemisphere snow cover to a changing climate. *J. Clim.* **22**, 2124–2145 (2009).
39. Slivinski, L. C. et al. Towards a more reliable historical reanalysis: Improvements for version 3 of the Twentieth Century Reanalysis system. *Quart. J. R. Meteorol. Soc.* **145**, 2876–2908 (2019).
40. Hersbach, H. et al. The ERA5 global reanalysis. *Q. J. Roy. Meteor. Soc.* **146**, 1999–2049 (2020).
41. Skamarock, W. C. et al. A Description of the Advanced Research WRF Version 4 Technical Note NCAR/TN-556+STR. *Mesoscale and Microscale Meteorology Division*. (National Center for Atmospheric Research, 2019).
42. Meinshausen, M. et al. Historical greenhouse gas concentrations for climate modelling (CMIP6). *Geosci. Model Dev.* **10**, 2057–2116 (2017).
43. Riahi, K., Grübler, A. & Nakicenovic, N. Scenarios of long-term socio-economic and environmental development under climate stabilization. *Technol. Forecast. Soc. Change* **74**, 887–935 (2007).
44. Eyring, V. et al. Overview of the Coupled Model Intercomparison Project Phase 6 (CMIP6) experimental design and organization. *Geosci. Model Dev.* **9**, 1937–1958 (2016).
45. Miguez-Macho, G., Stenchikov, G. L. & Robock, A. Spectral nudging to eliminate the effects of domain position and geometry in regional climate model simulations. *J. Geophys. Res.* **109**, D13104 (2004).

Acknowledgements

D.I.C. is supported by the European Space Agency (ESA) grant no. 4000136272/21/I-EF (CCN. N.1), 4DMED Hydrology. M.L.C. is supported by a postdoctoral contract from the program named “Programa de ayudas de apoio á etapa inicial de formación posdoctoral (2022)” funded by Xunta de Galicia (Government of Galicia, Spain). Reference number: ED481B-2022-055. M.S.R. and G.M.M. acknowledge support from the Spanish Ministry of Science and Innovation RIESPIRO (PID2021-128510OB-I00). M.d.C.L. acknowledges funding from the European Union’s Horizon 2020 research and innovation program under grant agreement No 101037193 (I-CHANGE project). D.G.M acknowledges support from the European Research Council (HEAT, 101088405). Computation took place at CESGA (Centro de Supercomputación de Galicia), Santiago de Compostela, Galicia, Spain.

Author contributions

D.I.C. designed the experiment, performed the simulations, created the figures, and wrote the first manuscript draft. M.L.C. was in charge of the analog analysis and the corresponding figures (Figs. 2 and 3). J.J.G.A. provided the snow observation data from AEMET and created the corresponding figure (Fig. 1d). M.L.C and J.J.G.A. also collaborated in writing the article. M.S.R., M.d.C.L., G.M.M., and D.G.M. contributed with ideas, interpretation of the results, and manuscript revisions.

Competing interests

The authors declare no competing interests.

Additional information

Supplementary information The online version contains supplementary material available at <https://doi.org/10.1038/s43247-024-01503-7>.

Correspondence and requests for materials should be addressed to Damián. Insua-Costa.

Peer review information *Communications Earth & Environment* thanks Andrés Merino and the other, anonymous, reviewer(s) for their contribution to the peer review of this work. Primary Handling Editors: Alireza Bahadori and Aliénor Lavergne. A peer review file is available.

Reprints and permissions information is available at <http://www.nature.com/reprints>

Publisher’s note Springer Nature remains neutral with regard to jurisdictional claims in published maps and institutional affiliations.

Open Access This article is licensed under a Creative Commons Attribution 4.0 International License, which permits use, sharing, adaptation, distribution and reproduction in any medium or format, as long as you give appropriate credit to the original author(s) and the source, provide a link to the Creative Commons licence, and indicate if changes were made. The images or other third party material in this article are included in the article’s Creative Commons licence, unless indicated otherwise in a credit line to the material. If material is not included in the article’s Creative Commons licence and your intended use is not permitted by statutory regulation or exceeds the permitted use, you will need to obtain permission directly from the copyright holder. To view a copy of this licence, visit <http://creativecommons.org/licenses/by/4.0/>.

© The Author(s) 2024